A Simplified Sub-grid Parameterization for Volcanic Aerosol Injections of the Stratosphere in E3SMv2 in Support of the DOE CLDERA Project

Joe Hollowed

Preliminary Exam Research Prospectus

July 2022

Abstract

This paper describes the design and implementation of stratospheric aerosol injection (SAI) events in an idealized configuration of the Department of Energy's (DOE) Energy Exascale Earth System Model (E3SMv2). These aerosols are implemented as "tracers" within the framework of the climate model, i.e. dimensionless mixing-ratio quantities which are advected with the winds by the model's transport scheme. The spatio-temporal description of the injected tracer species, as well as their chemical interaction and evolution, are encoded as sub-grid parameterizations via a set of simple ODEs. The form of the equations are designed to mimic materials characteristic of stratospheric volcanic eruptions, specifically those chemical species which are known to perturb the Earth system's energy balance, and thus climate. Here we employ highly-simplified expressions of these processes in the absence of almost all other diabatic forcings normally present in a coupled-climate model. Future work will include the establishment of our model's output products as validation datasets for the climate source-impact attribution methods currently being developed by the DOE's CLDERA project, where they will serve as a plausible representation of geoengineering activities. We also plan to continue with the implementation of more tracers and methods in support of this project, and to asses E3SMv2's representation of the general circulation, specifically stratospheric structures and stratosphere-troposphere exchange, and how they respond to aerosol forcings.

1 Overview

The atmosphere of Earth is in a constant communication with itself, exchanging energy across space, time, and wide spectral ranges through the complex interplay of surface turbulence, wave excitation and eventual breaking, meandering jets and vortexes, and dramatic wind oscillations high above the ground. Feedbacks from moisture, chemical substances, and solar radiation are capable of meddling in all of these dynamics, and the coupling of this fantastic system with processes of the ocean and continents provides irregular climate responses.

Since the advent of Atmospheric General Circulation Models (AGCMs) in the 1960's, both their conceptual and computational complexity has steadily increased to the point of today's sophisticated Earth System Models (ESMs) (Randall, 2010), which are capable of estimating climate evolution of a coupled ocean-atmosphere system at timescales and resolutions taking advantage of machines approaching the exascale. The societal impacts of these model developments, which have allowed predictive power for both weather and climate change, cannot be understated.

So trustworthy have these ESMs become, that they are now the primary laboratories for experiments of potentially viable *geoengineering* activities, i.e. efforts of Earth system manipulation aimed at climate change mitigation, or even reversal. For example, the Stratospheric Aerosol Geoengineering Large Ensemble Project (GLENS) has recently employed a 20-member ensemble of coupled ESM simulations with comprehensive middle-atmosphere chemistry (Tilmes et al., 2018). The project strives to asses the efficacy, and side effects, of "albedo enhancement" geoengineering solutions, which propose the controlled emission of sulfur aerosols into the stratosphere. These aerosols increase Earth's albedo by a direct (scattering of solar radiation) and indirect effect (cloud nucleation encouragement), which counteracts anthropogenic greenhouse warming (Crutzen, 2006).

While these experiments are currently only preformed in computer models, other projects such as China's "Sky River" cloud-seeding campaign are already underway (Watts, 2020), which suggests a current disincentive to consider spatially-distant consequences in the development of such geoengineering activities. Through efforts such as the GLENS project, it has been established that the unintended climate side-effects of these activities are numerous (Tilmes et al., 2018), and thus, warming-based metrics are insufficient criteria in their design; we will also need to have established methods of identifying *all* downstream climate impacts of mitigation activities, even indirect ones.

The DOE's brand new CLDERA project (*CLimate impact: Determining Etiology thRough pAthways*) lead at Sandia National Laboratory (SNL) has been designed to serve exactly this purpose. In the CLDERA project proposal, it is suggested that our current inability to both assess climate impacts and *scientifically attribute* them to particular actions will inevitably hamper relevant policy decisions. In particular, it is emphasized that scientific policy motivations can only be given in the case that we are able to attribute predicted climate impacts fractionally to the degenerate effects of: the mitigation activity itself, anthropogenic climate change, and natural climate variability. This stands in contrast to previous studies (e.g. GLENS) which operate by running sufficiently large ensembles to allow robust correlations to be measured, rather than detecting the actual physical sequence of events from source to impact.

To this end, the CLDERA approach is centered around the concept of "pathways", defined as the etiological chains of physical processes that connect source events to climate impacts, and their spatio-temporal evolution. It is hypothesized that the identification and tracking of these pathways in simulated and observational datasets will assist in *ranking* the dominance of various source events for a given impact. In the development of the methods that will be required for these determinations, and testing of the pathway hypothesis, CLDERA will use the 1991 eruption of Mt. Pinatubo (and the subsequent observed climate anomalies) as an exemplar. This stratospheric aerosol injection (SAI) event deposited ~15-20 Tg of SO_2 into the atmosphere, and was associated with subsequent local stratospheric warming, as well as surface cooling over the following 2-3 years (McCormick et al., 1995).

Our group, the Atmospheric Dynamics Modelling Group (ADMG) at the University of Michigan (UM), are contributing to this effort through the development of a simplified SAI model within an idealized atmospheric configuration that we have embedded inside the DOE's Energy Exascale Earth System Model (E3SM). Our model allows the advection of at least three new tracers species (SO_2, volcanic ash, and sulfate aerosol) which serve as the inputs to local sub-grid heating parameterizations of the atmosphere. This heating does not require mediation by any chemistry or radiation packages, and the SO_2-to-sulfate conversion is defined directly by a coupled set of ODE's.

Our model will serve as an important keystone in the CLDERA project's "tiered verification and validation" approach to development. This approach dictates that the forthcoming pathway discovery and impact attribution methods should be validated against a series of data products of increasing complexity, starting from one-dimensional synthetic time series, and ending in fully-coupled ESM model runs with complex physics parameterizations. Our model sits between these two extremes.

Through the remainder of this section, we describe the in more detail the 1991 eruption of Mt. Pinatubo, and the E3SM model. In Section 2, we describe our injection model, as well as the idealized Held-Suarez-Williamson (HSW) climatology within which it is embedded. Section 2.3 discusses preliminary results from the model as implemented in E3SMv2. In Section 3, future work is discussed, and Section 4 gives a summary.

1.1 1991 eruption of Mt. Pinatubo

The eruption of the stratovolcano Mt. Pinatubo started on June 15, 1991 in western Luzon, Phillipines near 15 °N. Particularly relevant to the climate impacts of this eruption was the injection of sulfur species into the stratosphere, namely sulfur dioxide (SO_2), and its subsequent reaction product, *sulfate aerosol* (a combination of H_2O and H_2SO_4 (sulfuric acid)). Also present was an enormous amount of ash, ice, and water vapor.

The radiative forcing associated with the stratospheric presence of these aerosols created a net climate response featuring ozone depletion in the polar regions, warming of the lower stratosphere by absorption of upward travelling longwave radiation, and surface cooling in the tropics by scattering of incoming solar radiation, and thus an increase in the average aerosol optical depth (AOD) (Robock, 2002; Robock, 2000). The mean tropospheric temperature in 1992 was measured to be 0.7 °C lower than from 1991, and stratospheric warming peaked in September of 1991 with anomalies of 3.5 K (McCormick et al., 1995).

This event has been chosen as the exemplar for CLDERA to test its hypothesis, and base it's initial development on, for the following reasons:

1. The source is exogenous to the Earth System, and therefore there is no specific need to achieve accuracy in the initial state.
2. The eruption was sufficiently large to cause climate anomalies which exceed internal variability of the system.
3. It is the most well-observed SAI event in recent history, and many data sources are available (e.g. refer-

ences in Table 1).

4. A well-characterized system with a strong climate-impact signal will be promising for the verification and validation of automatic detections and rankings of source-impact pathways.

5. Geoengineering events are the ultimate scientific target of CLDERA, and this natural SAI event is closely related to the geoengineered sulfate emission interventions discussed in Section 1.

It is hoped that the Mt. Pinatubo eruption will be able to serve as a "ground truth" against which the pathway discovery and attribution methods can be tested. This will especially be true if the climatic effects of the eruption can be reproduced in a simulation for which all *other* sources of anomalous radiative forcings can be manually removed (i.e. the focus of this report, discussed in Section 2).

1.2 The DOE E3SM model

The DOE's E3SM coupled climate model includes independent components describing evolution of the atmosphere, ocean and sea ice, land, and river transport; energy exchanges between these components are mediated by a "coupler" which coordinates the communication. The model was initially born as a fork of the popular Community Earth System Model (CESM) version 2 (Danabasoglu et al., 2020) for the Accelerated Climate Modeling for Energy (ACME) project, the goal of which is to enable and optimize the use of DOE laboratory computing resources for Earth system modeling at extreme scale (Bader et al., 2014).

Throughout the remainder of this report, we will mainly discuss the atmospheric component, the E3SM Atmosphere Model (EAMv2) (Golaz et al., 2022), which consists of a dynamical core (or "dycore") and various physical parameterizations (or "sub-grid physics") for turbulence, clouds, deep convection, radiation, atmospheric chemistry and aerosols. For our purposes, we use a dry, idealized configuration of EAMv2, which deactivates all of these physical parameterizations and replaces them with idealized expressions (see Section 2.1).

The dycore solves the shallow-atmosphere, hydrostatic equations of motion on a rotating sphere, implemented in the Higher Order Method Modeling Environment (HOMME) (Dennis et al., 2012) which uses a spectral finite element method on a cubed-sphere horizontal discretization. The 72-level vertical discretization uses a terrain-following pressure coordinate with a model top at ~60 km, and the timestepping algorithm is a 3rd-order accurate Runge-Kutte method (Golaz et al., 2022). The sub-grid physics use a separate grid than the dynamics, which requires a "remap" algorithm to exchange information between the grids at the timestep (Hannah et al., 2021).

Of particular relevance to the work presented here is the model's tracer transport method, which uses a new interpolation semi-Lagrangian (ISL) approach (Bradley et al., 2021), and boasts mass-tracer consistency, mass conservation, shape preservation, and allows for accuracy even with long timesteps (compared to the timestep Δt of the dynamics).

2 The idealized SAI model

In this section we describe our SAI model, which produces SO_2, sulfate, and ash mixing-ratios which are driven by simple analytic relationships that replace more standard (and complicated) chemistry and radiative packages. In designing the terms appearing in these analytic forms, we are able to control the number of "nodes" (or cause-effect pairs) appearing in pathways like e.g. the aerosol direct effect which drive temperature anomalies. In this way, we say that we have inserted *analytic pathways* into the output datasets, which will serve as a "ground truth" for CLDERA validation studies.

We also choose to minimize all other diabatic effects in the atmosphere as much as possible; the injection event is embedded in a dry setting with flat topography, where the climatology arises from an idealized Held-Suarez-Williamson (HSW) forcing, which replaces all turbulence, radiative, and moist convective parameterizations with a linear temperature relaxation to a prescribed equilibrium profile, and dissipation of surface winds via Rayleigh damping. This is done for simplicity so that the analytic pathways may still be well-characterized, but also for computational affordability which will easily allow ensemble studies. The details of the SAI parameterizations and the HSW forcing are given in Sections 2.1-2.2.

2.1 Held-Suarez-Williamson climatology

Held and Suarez (1994) (hereafter HS94) originally proposed a benchmark calculation designed for the intercomparison of modular dynamical cores of AGCMs, which provides Rayleigh damping of low-level winds to represent friction at the boundary layer, and a Newtonian temperature relaxation toward an analytic profile which is

a function of latitude and pressure. Many other dycore inter-comparison test protocols exist (e.g. Jablonowski and Williamson (2006)), though the HS94 forcing was specifically meant to facilitate assessments of statistically steady states in climate produced by the dycore after long timescales (for which the true solution is unknown).

Williamson et al. (1998) (hereafter HSW98) later noted that the HS94 benchmark would not be applicable to their dycore inter-comparison studies of tropopause formation, since it deliberately maintains a "passive" stratosphere, supporting none of the typical stratospheric structures such as the polar jets. To remedy this, they provide a modification of the original HS94 temperature equilibrium profile, which includes realistic lower-stratospheric lapse rates in the tropics and polar regions. We call this forcing the Held-Suarez-Williamson (HSW) configuration. In our simulations, we use the HSW forcing, and omit all other moist convective, radiative, turbulence descriptions. However, the standard E3SMv2 model top sits at ~60 km, or ~0.1 hPa, well above the model top of HSW98 at ~3 hPa. Applying the temperature relaxation profile as published in HSW98 to E3SMv2 therefore results in undesired reversals in the polar lapse rate at 2 hPa, as well as temperatures at the tropical model top in excess of 300 K (while observed monthly-mean zonal-mean temperatures peak at ~260 K near 50 km in the tropics (Holton and Hakim, 2013b)).

We choose to avoid these artifacts by forcing the lapse rate to zero above $p_{\rm pl} = 2$ hPa, i.e. the equilibrium profile $T_{\rm eq}$ becomes constant with respect to height at pressures smaller than $p_{\rm pl}$, taking the form

$$T_{\rm eq} = T_0 \left[\min\left(1, \frac{p^*}{p_d}\right) \right]^{\frac{R\gamma_d}{g}} + T_0 \left[\left[\min\left(1, \frac{p^*}{p_i}\right) \right]^{\frac{R\gamma_i}{g}} - 1 \right] \tag{1}$$

where

$$p^* = \max\left(p, p_{\rm pl}\right) \tag{2}$$

and

$$p_i = p_{\rm eq} - (p_{\rm eq} - p_{\rm pl}) \frac{1}{2} \left[1 + \tanh\left(A\left[|\phi| - \phi_0\right]\right)\right] \tag{3}$$

Here, $p_d = p_{\rm eq} = 100$ hPa, below which the original HS94 formulation applies. Above this, the temperature decreases with constant lapse rate $\gamma_d = 2$ K/km, until $p \le p_i$, where a temperature is added that increases with constant lapse rate $\gamma_i = -3.345$ K/km. The remainder of the parameters are set to the values presented in HSW98 and HS94.

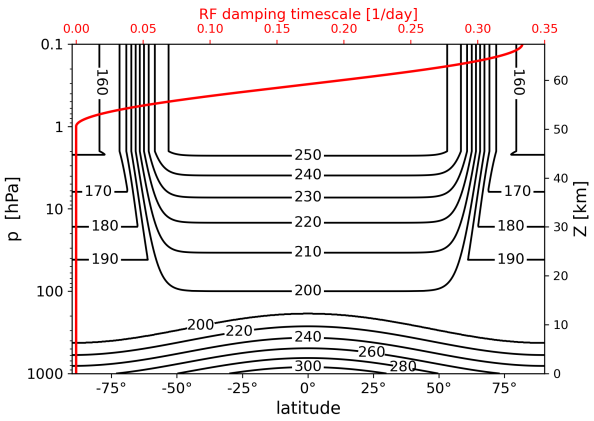

Figure 1: *The HSW98 temperature equilibrium profile T_{eq} with our "extended stratopause" modification. The solid red line shows the Rayleigh friction profile Eq.5, with values read off of the top (red) axis.*

We attempted to follow the advice of the HSW98 authors by lowering the parameter $p_{\rm pl}$ from 2 hPa to something coincident with the E3SMv2 model top; while this does change the structure of the relaxation profile to better resemble that of HSW98, it does nothing to address the unrealistic temperatures at the model top. By replacing $p \to p^*$ as was done in Eq.(1), the profile for $p \le 2$ hPa is just

$$T_{\rm eq} = T_0 \left(\frac{p_{\rm pl}}{p_d}\right)^{R\gamma_d/g} + T_0 \left[\left(\frac{p_{\rm pl}}{p_i}\right)^{R\gamma_i/g} - 1 \right] \tag{4}$$

which imposes a sort of "extended stratopause".

In addition, we include a second Rayleigh damping mechanism, similar to the HS94 treatment of the surface friction, near the model top as a "sponge layer" for calming the polar jet winds and absorbing spurious wave reflections, as described in Jablonowski and Williamson (2011). The vertical profile that we choose for the damping strength follows the implementation of Lin et al. (2017), and has a monotonic onset from ~100 Pa to the model top:

$$k(p) = k_0 \sin\left(\frac{\pi}{2} \frac{\log(\eta_c/\eta)}{\log(\eta_c/\eta_T)}\right)^2 \tag{5}$$

Here, the normalized pressure coordinate is $\eta \equiv p/p_0$, with $p_0 = 1000$ hPa. We define an onset position at $\eta_c = (1\,\text{hPa})/p_0$, and the normalized pressure at the model top as $\eta_T \equiv p_{\rm top}/p_0$. The maximum strength of the damping is set via $k_0 = 1/(3$ days). Given Eq.(1) and Eq.(5),

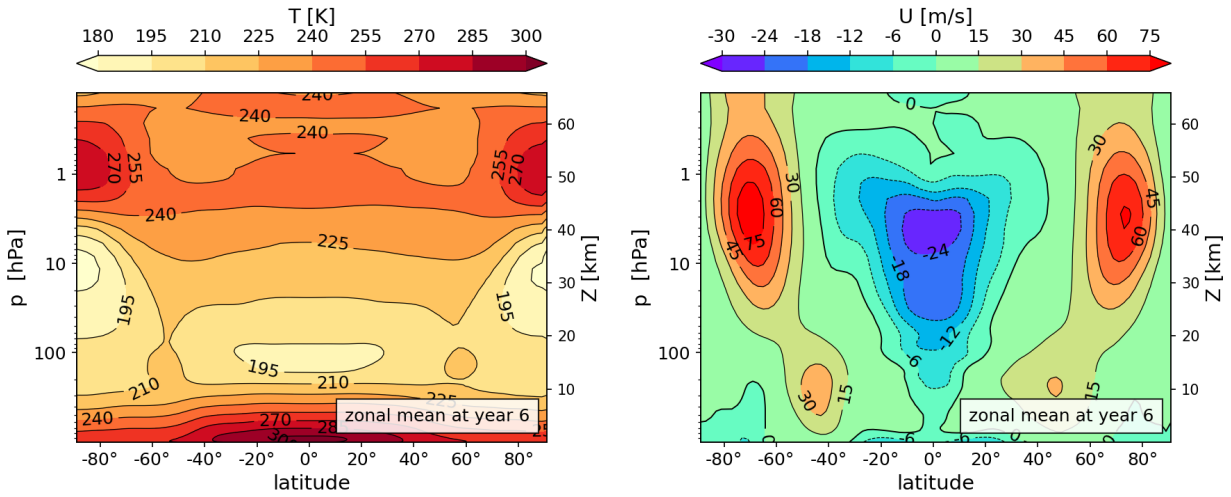

Figure 2: *Instantaneous temperature and zonal wind fields from E3SMv2 after a 6-year integration subject to our modified HSW forcing as outlined in Section 2.1. The spatial discretization is the "ne16pg2" spectral element grid, which gives approximately a 2-degree resolution, and the vertical discretization is the E3SMv2 default with 72 levels to 60 km. We use a physics timestep of* $\Delta t = 1800$ *s. See text for interpretation.*

the wind and temperature tendencies will be updated at each physics timestep by

$$\frac{\partial T}{\partial t} = -k_T(\phi, p)\left(T - T_{\text{eq}}\right) \tag{6}$$

$$\frac{\partial \vec{v}}{\partial t} = \left(-k(p) - k_v(p)\right)\vec{v} \tag{7}$$

where k_T and k_v are the relaxation and damping timescales for T and surface $\vec{v}$, respectively, defined in HS94.

Figure 1 shows our modified HSW equilibrium temperature profile as well as the employed vertical profile for the sponge layer damping, and Figure 2 shows zonal-mean instantaneous temperature and zonal wind fields resulting from a 6-year spinup period using these forcings in E3SMv2 with an approximately 2-degree spatial resolution (ne16 SE grid), 72 vertical levels to 60km, and physics timestep of $\Delta t = 1800$ s. This is also the snapshot used as the initial condition for the SAI runs that are discussed in Section 2.2. The temperature structure in the stratosphere is quasi-realistic, reaching maximum tropical stratospheric temperatures of ~240 K (slightly cooler than observed). Temperature minima are seen near the tropical tropopause, as well as the polar middle-stratosphere. Sharp vertical temperature gradients are seen near our "stratopause" in the polar regions, leading to temperatures in excess of 270 K. In the zonal wind, we see the formation of tropospheric mid-latitude westerly jets with maximum wind speeds of ~30 m/s, and strong stratospheric polar jets of up to ~75 m/s. Easterlies up to -30 m/s dominate the tropical stratosphere. Again, there is no seasonality present, and by the features just described, each hemisphere varies about a winter-like steady state.

2.2 Tracer injection

The tracer injection occurs uniformly over a single model column i^*. This means that the initial tracer *densities* will change based on the choice of horizontal grid, as we choose to directly model the *mass* tendency of each tracer j:

$$\frac{\partial m_j}{\partial t} = R(m_j) + f \tag{8}$$

where $R(m)$ is an exponential removal function with e-folding timescale $1/k_j$,

$$R(m_j) = -k_j m_j \tag{9}$$

and f is a source term which describes the injection of an aerosol mass into the column

$$f = A_j V(z) T(t) \delta_{i,i^*} \tag{10}$$

with separable temporal and vertical dependencies $T(t)$ and $V(z)$, where z is geometric height. The Kronecker-Delta function δ_{i,i^*} simply selects the desired column i^*

($\delta_{i,i^*} = 0$ for $i \neq i^*$), with i^* chosen by minimizing the great circle distance

$$r(\phi_i, \lambda_i) = a\cos^{-1}\left[\sin\phi_i \sin\phi_0 + \cos\phi_i \cos\phi_0 \cos(|\lambda_i - \lambda_0|)\right] \tag{11}$$

with respect to the desired injection location latitude ϕ_0 and longitude λ_0. The time dependence is taken to be a simple step function, representing a constant injection for a time t_f, after which the source vanishes,

$$T(t) = \begin{cases} 1 & \text{if } t \leq t_f \\ 0 & \text{if } t > t_f \end{cases} \tag{12}$$

The source function for tracer j is normalized by the constant A_j, which scales the *total injected mass* to a known parameter M_j, by

$$M_j = f t_f = A_j t_f V(z) \delta_{i,i^*} \tag{13}$$

In deriving A_j, we first discretize the function V on vertical levels k. If instead this constant is derived from the continuous expression, we may lose some of the total mass to numerical diffusion once the mass distribution is deposited onto the model grid. The discretized forms for the mass tendency and total mass are

$$\frac{\partial m_{j,i,k}}{\partial t} = -k_j m_j + A_j V(z_k) \delta_{i,i^*}, \tag{14}$$

$$M_j = \sum_k A_j t_f V(z_k) \delta_{i,i^*} \tag{15}$$

$$\implies A_j = \frac{M_j}{t_f \sum_k V_k} \frac{\text{kg m}}{\text{s}} \tag{16}$$

Here, we have discarded the delta function from the result to avoid a division by zero in the case that $i \neq i^*$, justified by the fact that injection is already constrained to vanish under this condition by the presence of δ_{i,i^*} in the tendency $\partial m_j / \partial t$. We have also defined $V_k \equiv V(z_k)$.

The vertical dependence is modeled as a skew-normal distribution as described in Sheng et al. (2015)

$$g(z) = \frac{2}{\sqrt{2\pi}\sigma} \exp\left(-\frac{(z-\mu)^2}{2\sigma^2}\right) \int_{-\infty}^{\alpha \frac{z-\mu}{\sigma}} \frac{1}{\sqrt{2\pi}} e^{-\frac{x^2}{2}} dx \tag{17}$$

$$= \frac{1}{\sqrt{2\pi}\sigma} \exp\left(-\frac{(z-\mu)^2}{2\sigma^2}\right) \left[1 - \text{erf}\left(\alpha \frac{\mu - z}{\sqrt{2}\sigma}\right)\right] \tag{18}$$

which is truncated on the injection bounds $z_{\min}, z_{\max}$ such that

$$V(z) = \begin{cases} g(z) & \text{if } z_{\min} \leq z \leq z_{\max} \\ 0 & \text{otherwise} \end{cases} \tag{19}$$

The location parameter μ gives the vertical position of the peak injection in the case of no skewness. The skewness is controlled by the parameter α, which drives the peak to higher altitudes for $\alpha > 0$, and lower altitudes for $\alpha < 0$. Finally, the scale parameter σ determines the amount of dispersion about the peak. Choices for these parameters are given in Table 1, which correspond to configurations `R001` and `R033` of Sheng et al. (2015). There, the authors take one further step by instead using as the vertical profile $G(z) \equiv g(z) / \int_{z_{\min}}^{z_{\max}} g(z)$, which normalizes $g(z)$ to unit area within the truncation bounds. We do not do this, and instead allow this normalization to be implicitly folded into the computation of A (in effect, we replace their integration of $g(z)$ with the sum $\sum_k V_k$).

Rather than $\partial m_j / \partial t$ itself, the quantity ultimately required by EAMv2's physics interface is the tendency of the tracer *mixing ratio* $q_j \equiv m_j / m_{\text{atm}}$. Given the derivations above, this is

$$\frac{\partial q_{j,i,k}}{\partial t} = \frac{1}{m_{\text{atm},i,k}} \left[-k_j m_j + \frac{M_j}{t_f \sum_k V_k} V_k \delta_{ii^*}\right] \tag{20}$$

The air mass m_{atm} can be replaced by

$$m_{\text{atm},i,k} = \rho_{i,k} a_i \Delta z_k \tag{21}$$

where $\rho_{i,k}$ is the air density in this grid cell, a_i is the column area, and Δz_k is the height of the vertical level. This is further reduced to a function of nothing but the model level pressure thickness Δp_k via the hydrostatic approximation:

$$\frac{\Delta p_k}{\Delta z_k} + \rho_{\text{atm},i,k} g = 0 \tag{22}$$

$$\implies \rho_{\text{atm},k} \Delta z_k = \frac{\Delta p_k}{g} \tag{23}$$

$$\implies m_{\text{atm},i,k} = \frac{\Delta p_k a_i}{g} \tag{24}$$

(the sign is discarded from the first to second line, since this only communicates that p decreases with z, and what we care abut is the magnitude. Consider it a "flip of integration bounds").

The final expression for the update of tracer j at position (i, k) is then

$$\frac{\partial q_{j,i,k}}{\partial t} = \frac{g}{\Delta p_k a_i} \left[-k_j m_j + \frac{M_j}{t_f \sum_k V_k} V_k \delta_{ii^*}\right] \tag{25}$$

for $z \in [z_{\min}, z_{\max}]$ and $t \in [0, t_f]$.

We use this framework to describe the simultaneous injection of tracers j for the set $j \in \{\text{SO}_2, \text{sulfate, ash}\}$. Observations giving the total injected mass and e-folding time

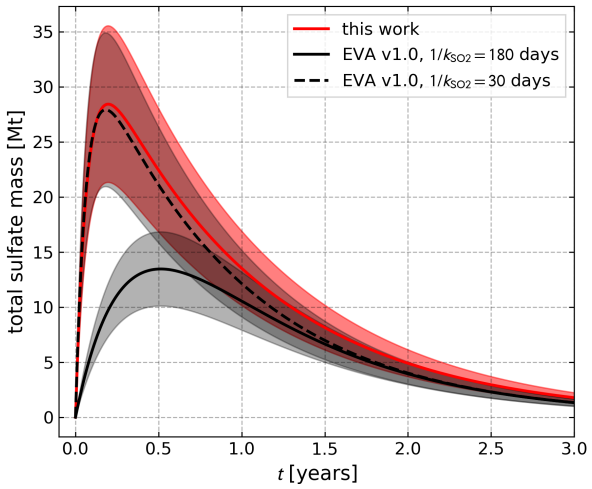

Figure 3: *Total sulfate mass time series from the analytic solutions of our model (red solid line), and those from EVA v1.0 with* $1/k_{SO2} = 180$ *days (their default; solid black line), and an adjustment* $1/k_{SO2} = 30$ *days (our default; dashed black line). The adjustment of this parameter fully explains the difference in the peak mass, and all curves begin to converge after 1 year. The red curve remains largest in mass value since our e-folding timescale of sulfate (360 days) is longer than EVA v1.0 (330 days). The bands about each curve are* $\pm 25\%$ *of the mass value, which is the approximate uncertainty in the (Guo, Bluth, et al., 2004) measurement of the inital* SO_2 *loading.*

for each species were estimated from satellite data and published in Guo, Rose, et al. (2004), Guo, Bluth, et al. (2004), and Barnes and Hofmann (1997). Table 1 gives the parameter values chosen for this work, in which case the model describes the 9-hour injection of a plume extending from 17km to 30km in the vertical. We assume no background values for any of the injected species prior to the eruption, as in some other studies (e.g. Bekki and Pyle (1994)). Figure 5 shows an analytic advection-free solution to the problem (described in Section 2.2.4). Sections 2.2.1-2.2.3 describe the methods by which the tracers can be made "active", providing feedback to the prognostic fields of the model in a way designed to represent simplified causal pathways.

2.2.1 Sulfate formation via "toy chemistry"

Once injected into the atmosphere, SO_2 follows an oxidation chain with an end product of sulfuric acid (H_2SO_4) that condenses with water vapor to form sulfate aerosol particles (Bekki, 1995). This aerosol has a removal timescale of one year (Barnes and Hofmann, 1997), much longer than SO_2, and is responsible for much of the heating that perturbs the Earth's energy balance and atmospheric circulation after a stratospheric volcanic eruption (McCormick et al., 1995; Robock, 2002).

In climate models with high-complexity, this process is mediated by chemistry, radiation, and moist sub-grid processes. Here, we replace all of this by a direct, analytic coupling from SO_2 to sulfate, in a way inspired by the so-called "toy chemistry" of Lauritzen et al. (2015). The SO_2 sink $R(m_{SO2})$ retains the form of Eq.(9) and e-folding time k_{SO2}, but is now viewed as a reaction rate which provides a sulfate source.

The sulfate tendency mass is therefore

$$\frac{\partial m_{\text{sulfate}}}{\partial t} = -k_{\text{sulfate}} m_{\text{sulfate}} + w k_{SO2} m_{SO2} \tag{26}$$

Here, the reaction weight w encodes the net production of sulfate per unit mass of SO_2.

In practice, w can be a tuning parameter of the model, but we can inform a first choice for it from chemistry. Since the overall effect of the oxidation sequence yields one aerosol "particle" of sulfate per molecule of SO_2 (Bekki, 1995), w will just be the ratio of the sulfate to SO_2 molar mass. It is known from observation that sulfate particles vary in their composition across latitude, altitude, and season (Yue et al., 1994), dependent on availability of water vapor, and temperature. In principle, this should complicate a realistic choice of w. We make the simplifying assumption that all sulfate particles are 75% H_2SO_4 by mass, as in Bekki (1995), and suggested by observation (Rosen, 1971; Yue et al., 1994). Defining this percentage as $f_{\text{acid}} = 0.75$, and the molar masses of H_2SO_4 and SO_2 as w_{H2SO4} and w_{SO2}, the reaction weighting is

$$w = \frac{w_{H2SO4}/f_{\text{acid}}}{w_{SO2}} \approx \frac{1/0.75 \times 98.079 \text{ g/mol}}{64.066 \text{ g/mol}} \approx 2.04 \tag{27}$$

In the analytic (advection-free) solution to the tracer evolution described in Section 2.2.4, this choice of w results in a peak sulfate mass of about ~28 Mt occuring ~2 months after injection. This is consistent with previous modeling efforts by e.g. Bluth et al. (1997). In that study, however, the authors note that the observed AOD anomalies post-Pinatubo lagged behind the sulfate loading, in the case that the sulfate production is modeled as a direct consequence of SO_2 depletion.

Toohey et al. (2016) (hereafter EVA v1.0) also model the $SO_2 \rightarrow$ sulfate conversion directly, but show that the sul-

fate mass and AOD peaks can be matched in time by tuning $k_{SO2} = 1/180$ days^{-1} . This differs markedly from the measured timescale of the post-Pinatubo SO_2 removal (Guo, Bluth, et al., 2004) of ~$1/25$ days^{-1} ; the claim is that this modified e-folding time is representing the *net* timescale of the entire SO_2 oxidation chain that arrives at H_2SO_4, which explains the signal lag observed in Bluth et al. (1997). Under this condition, the recovered sulfate mass peaks at ~13 Mt after 6 months. In Figure 3, we show the analytic solution to the "pulse injection" of sulfate mass from EVA v1.0, with both their choice of k_{SO2}, and ours. This shows that the difference in peak sulfate mass of the two models is explained only by this parameter choice, and not the reaction normalization. We therefore suggest that k_{SO2} may be a good candidate for future CLDERA ensemble studies.

2.2.2 Diabatic heating of the stratosphere

The presence of SO_2 and sulfate in the stratosphere induces a diabatic heating to the temperature field by absorption of upward-propagating longwave radiation. After the Mt. Pinatubo eruption, this process resulted in a temperature anomaly of up to ~3-4 K, peaking near 50 hPa, driven by a maximum net temperature change at a rate of ~1 K/month during the initial period following the injection, and subsequent plateau for nearly a year (see Mills et al. (2016), Figure 2).

We model this very simply as an additive contribution to the temperature tendency, in the form of a heating rate Q_{strat}, and an associated heating rate per units mass m, s_{strat}:

$$s_{\text{strat}} \equiv \frac{Q_{\text{strat}}}{m} = \frac{q c_p \delta T_{\text{strat}}}{q^*} \tag{28}$$

$$\implies \frac{\partial T}{\partial t} = \ldots + \frac{q \delta T_{\text{strat}}}{q^*} \tag{29}$$

Here, the normalization constant q^* is left as a tuning parameter; see Table 1 and the discussion in Section 2.3. δT_{strat} is a constant temperature rate of change, and c_p is the specific heat of dry air at constant pressure. The dimensionless total tracer mixing ratio q is

$$q = \sum_{j \in S_1} q_j \tag{30}$$

where S_1 is the set of all tracers that are involved in the heating; by default, we use $S_1 = \{SO_2, \text{sulfate}\}$ (we allow ash to contribute no local heating). The ellipsis on the right-hand side of the Eq.(29) represents all other adiabatic and diabatic processes modifying the temperature field (e.g. the HSW forcing of Section 2.1).

2.2.3 Diabatic cooling of the surface by the AOD

Increased *aerosol optical depths* (AOD) decrease the flux density of shortwave solar radiation reaching the troposphere, and contributed to an observed surface cooling of ~2-3 K during the two years following the eruption of Mt. Pinatubo. A given aerosol species present in the atmosphere will contribute to "extinction" of solar radiation by both absorption and scattering (Petty, 2006), with a magnitude expressed via absorption and scattering coefficients β_a, β_s with dimensions of inverse volume. The combined effect of these processes give a single *extinction coefficient*

$$\beta_e \equiv \beta_a + \beta_s \tag{31}$$

The dimensionless *optical depth* or *optical thickness* $\tau(V)$ is a measure of the opacity of a particular volume element V, obtained by integrating the extinction:

$$\tau(V) \equiv \int_V \beta_e(x,y,z) dV' \tag{32}$$

We can express the extinction coefficient of all present aerosols as a superposition of each contributing species:

$$\beta_e = \sum_j \beta_{e,j} = \sum_j b_j \rho_j = \sum_j b_j q_j \rho_{atm} \tag{33}$$

where b_j is the *mass extinction coefficient* of the species, with dimensions of inverse mass (giving fractional extinction per unit mass), and ρ_j is the tracer mass density. The AOD at a height z with model top z_{top} is then computed via the definition Eq.(32) with the *parallel plane approximation* ($\beta_e(x,y,z) \approx \beta_e(z)$) by

$$\tau(z, z_{\text{top}}) = \int_{z'}^{z_{\text{top}}} a \beta_e(z) dz' \tag{34}$$

$$= \int_z^{z_{\text{top}}} \sum_j a b_j q_j(z') \rho_{atm}(z') dz' \tag{35}$$

where a is a constant from an implicit integration of the horizontal dimensions, and has units of area. When discretized onto a grid with pressure levels k and columns i with area a_i, and summed over all contributing constituents j, this becomes

$$\tau_{i,k} = \sum_j \sum_{k'<k} a_i b_j q_{j,k'} \rho_{\text{atm},k'} \Delta z'_k \tag{36}$$

$$= \sum_j \sum_{k'<k} a_i b_j \frac{q_{j,k'} \Delta p'_k}{g} \tag{37}$$

where $k' < k$ specifies the set k' of all levels *above* level k, and and we have assumed that the index k decreases toward the model top.The pressure weights were obtained

Table 1: *SAI model parameters*

Parameter	Value	Units	Description	Reference
ϕ_0	15.15	deg	meridional plume center	
λ_0	120.35	deg	zonal plume center	
μ	22.59	km	peak injection altitude	Sheng et al. (2015)
σ	4	km	width parameter of plume	Sheng et al. (2015)
α	-2	-	vertical skewness of plume	Sheng et al. (2015)
$z_{\min}$, $z_{\max}$	17, 30	km	vertical plume truncation limits[a]	Sheng et al. (2015)
t_f	9	hr	injection duration	Wolfe and Hoblitt (1998)
Tracer-specific parameters				
k_{SO2}	1/25	$1/\mathrm{day}$	e-folding time for SO2	Guo, Bluth, et al. (2004)
k_{sulfate}	1/360	$1/\mathrm{day}$	e-folding time for sulfate	Barnes and Hofmann (1997)
k_{ash}	1	$1/\mathrm{day}$	e-folding time for ash	Guo, Rose, et al. (2004)
M_{SO2}	1.7×10^{10}	kg	injected mass of SO2	Guo, Bluth, et al. (2004)
M_{ash}	5×10^{10}	kg	injected mass of ash	Guo, Rose, et al. (2004)
w	2.04	-	$SO_2 \rightarrow$ sulfate weighting	See Section 2.2.1
$\delta T_{\mathrm{strat}}$	0.35	K/day	stratospheric heating rate	Stenchikov et al. (1998)
q^*	0.7×10^{-7}	-	strat. heating normalization[b]	See Section 2.2.2
δT_{surf}	-0.012	K/day	surface cooling rate by AOD	Stenchikov et al. (1998)
τ^*	1×10^{6}	-	AOD normalization[b]	See Section 2.2.3
z_{AOD}	5	km	max. height of surface cooling	Stenchikov et al. (1998)
b_{SO2}	1	kg^{-1}	SO_2 mass extinction coeff.	See Section 2.2.3
b_{ash}	1	kg^{-1}	ash mass extinction coeff.	See Section 2.2.3
b_{sulfate}	1	kg^{-1}	sulfate mass extinction coeff.	See Section 2.2.3

[a] These vertical scale parameters are also consistent with observational estimates of the maximum plume height (Holasek et al., 1996; Self et al., 1993). See discussion surrounding section 4.6 of Guo, Rose, et al. (2004) and Sheng et al. (2015) section 3.2.

[b] The parameters q^* and τ^* were manually tuned to yield zonal-mean, time-mean from days 150-180, peak heating rates that qualitatively matched those presented in Stenchikov et al. (1998).

by the hydrostatic approximation as shown in Eq.(22)-(23).

In practice, we may want to restrict the application of the cooling to a certain "surface layer" bounded by some maximum height z_{AOD}. In that case, $\tau_{i,k}$ becomes

$$\tau_{i,k} = \begin{cases} \sum_j \sum_{k'>k} a_i b_j \frac{q_{j,k'} \Delta p'_k}{g} & \text{if } z_k < z_{\mathrm{AOD}} \\ 0 & \text{otherwise} \end{cases} \tag{38}$$

We also define a shorthand for the AOD at the surface as $\tau_i \equiv \tau(0, z_{\mathrm{top}})$. After summing over k for this case, we see that each remaining term is just the total column mass burden $M_{j,i}$ of aerosol j, scaled by the mass extinction coefficient b_j,

$$\tau_i = \begin{cases} \sum_j b_j q_j M_i = \sum_j b_j M_{j,i} & k = k\mathrm{surf} \\ 0 & \text{otherwise} \end{cases} \tag{39}$$

where M_i is the total air mass of the column, and k_{surf} is the lowest model level. Likewise, Eq.(38) is a "partial column burden" at level k, scaled by b_j.

In reality, b_j are functions of frequency ν. We choose to instead take these as constants, which either assumes that the extinction of the species has spectral uniformity, or that any radiation relevant to the heating process is monochromatic. Further, if we make the simple choice $b_j = 1\ \mathrm{kg}^{-1}$, then our expression for the AOD just reduces to the (total or partial) aerosol column burden $\sum_j M_{j,i}$ in value.

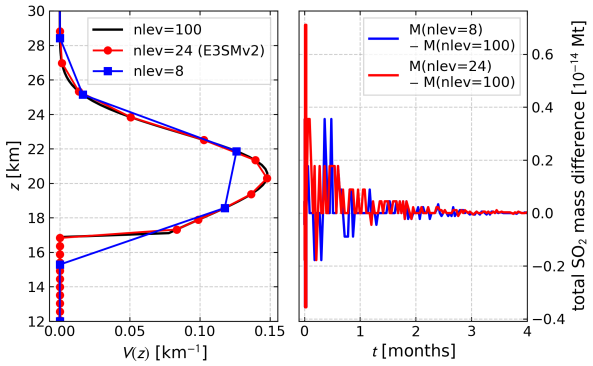

Figure 4: *Verification of the discretized form for the normalization constant A_{SO2} as defined in Eq.(16). Three vertical discretizations are shown with nlev levels distributed from 12 km to 30 km. The nlev= 24 curve gives the positions of the E3SMv2 levels in this region, where the z is the geopotential height above the surface as output from the model in the HSW configuration. (left) the sampling of the profile $V(z)$ (right) difference of the total SO2 mass across time between the nlev=8, 24 profiles, and a highly-resolved nlev=100 reference, computed via Eq.(43). The differences are on the order of machine precision.*

Finally, the surface cooling is modeled in a similar way to the stratospheric heating of Section 2.2.2:

$$s_{\text{surf}} \equiv \frac{Q_{\text{surf}}}{m} = \frac{\tau c_p \delta T_{\text{surf}}}{\tau^*} \tag{40}$$

$$\implies \frac{\partial T}{\partial t} = \ldots \frac{\tau \delta T_{\text{surf}}}{\tau^*} \tag{41}$$

where the normalization constant τ^* is analogous to q^* of Section 2.2.2, and is tuned in the same way. Default choices of these parameters are given in Table 1.

2.2.4 Analytic solutions in the absence of advection

In the absence of advection, the evolution of the tracer mass $m_j(t)$ in column i is solvable analytically, and the partial derivatives $\partial/\partial t$ used in the previous sections become material derivatives d/dt. Recall from Section 2 that for the fixed vertical position z', we have

$$\frac{dm_j}{dt} = -k_j m_j(t) + f(t), \tag{42}$$

Obtaining $m_j(t)$ is an initial-value problem of this first-order linear ODE for $m_j(t)$ with $m_j(0) = 0$. The solution is

$$m_j(t) = \frac{A_j V(z')}{k_j} e^{-k_j t} \left(e^{k_j t_{\min}} - 1 \right) \tag{43}$$

where we have defined

$$t_{\min} = \min[t, t_f] \tag{44}$$

Of course, any evaluation of this form will require a choice of vertical discretization to compute the normalization A_j.

This solution can be used to verify the sulfate formation implementation. In the absence of advection, and with the chocies $k_{\text{sulfate}} = 0$ and $w = 1$, Eq.(26) should give rise to a sulfate mass which reaches an enduring steady state equaling the total input SO_2 mass; let us call this quantity $\overline{m}_{\text{sulfate}}$. With these constraints, the total sulfur-species mass $m_{\text{SO2}}(t) + \overline{m}_{\text{sulfate}}(t)$ should be conserved once the injection is complete ($t > t_f$). The mass m_{SO2} is given by Eq.(43), which means

$$\begin{aligned} \frac{d}{dt}\overline{m}_{\text{sulfate}}(z,t) &= k_{\text{SO2}} m_{\text{SO2}} \\ &= A_{\text{SO2}} V(z) e^{-k_{\text{SO2}} t} \left(e^{k_{\text{SO2}} t_{\min}} - 1 \right) \end{aligned} \tag{45}$$

Integrating this (while keeping in mind to handle the piecewise inheritance from $t_{\min}$) gives the sulfate mass as

$$\overline{m}_{\text{sulfate}} = \frac{A_{\text{SO2}} V(k)}{k_{\text{SO2}}} e^{-k_{\text{SO2}} t} \left(1 - e^{k\text{SO2} t_{\min}} + e^{k_{\text{SO2}} t} k_{\text{SO2}} t_{\min} \right) \tag{46}$$

Taking $t_{\min} \to t_f$ allows us to verify the post-injection mass conservation:

$$\begin{aligned} & m_{\text{SO2}}(t) + \overline{m}_{\text{sulfate}}(t) \\ &= \frac{A_{\text{SO2}} V(z)}{k_{\text{SO2}}} e^{-k_{\text{SO2}} t} \left(e^{k_{\text{SO2}} t_f} - 1 \right) + \\ &\quad \frac{A_{\text{SO2}} V(k)}{k_{\text{SO2}}} e^{-k_{\text{SO2}} t} \left(1 - e^{k\text{SO2} t_f} + e^{k_{\text{SO2}} t} k_{\text{SO2}} t_f \right) \\ &= \frac{A_{\text{SO2}} V(k)}{k_{\text{SO2}}} e^{-k_{\text{SO2}} t} e^{k_{\text{SO2}} t} k_{\text{SO2}} t_f \\ &= A_{\text{SO2}} V(k) t_f = \text{const.} \end{aligned} \tag{47}$$

For completeness, the advection-free solution $m_{\text{sulfate}}(t)$ for arbitrary w and k_{sulfate} is

$$\begin{aligned} m_{\text{sulfate}}(t) = \frac{w A_{\text{SO2}} V(k)}{(k_{\text{sulfate}} - k_{\text{SO2}}) k_{\text{sulfate}}} e^{-k_{\text{sulfate}} t} \times \\ \left[k_{\text{SO2}} \left(1 - e^{k_{\text{sulfate}} t_{\min}} \right) - k_{\text{sulfate}} e^{(k_{\text{sulfate}} - k_{\text{SO2}}) t} \left(1 - e^{k_{\text{SO2}} t_{\min}} \right) \right] \end{aligned} \tag{48}$$

In Figure 5, the mass evolution of each tracer across time is shown in the injection column, given by Eq.(43) and

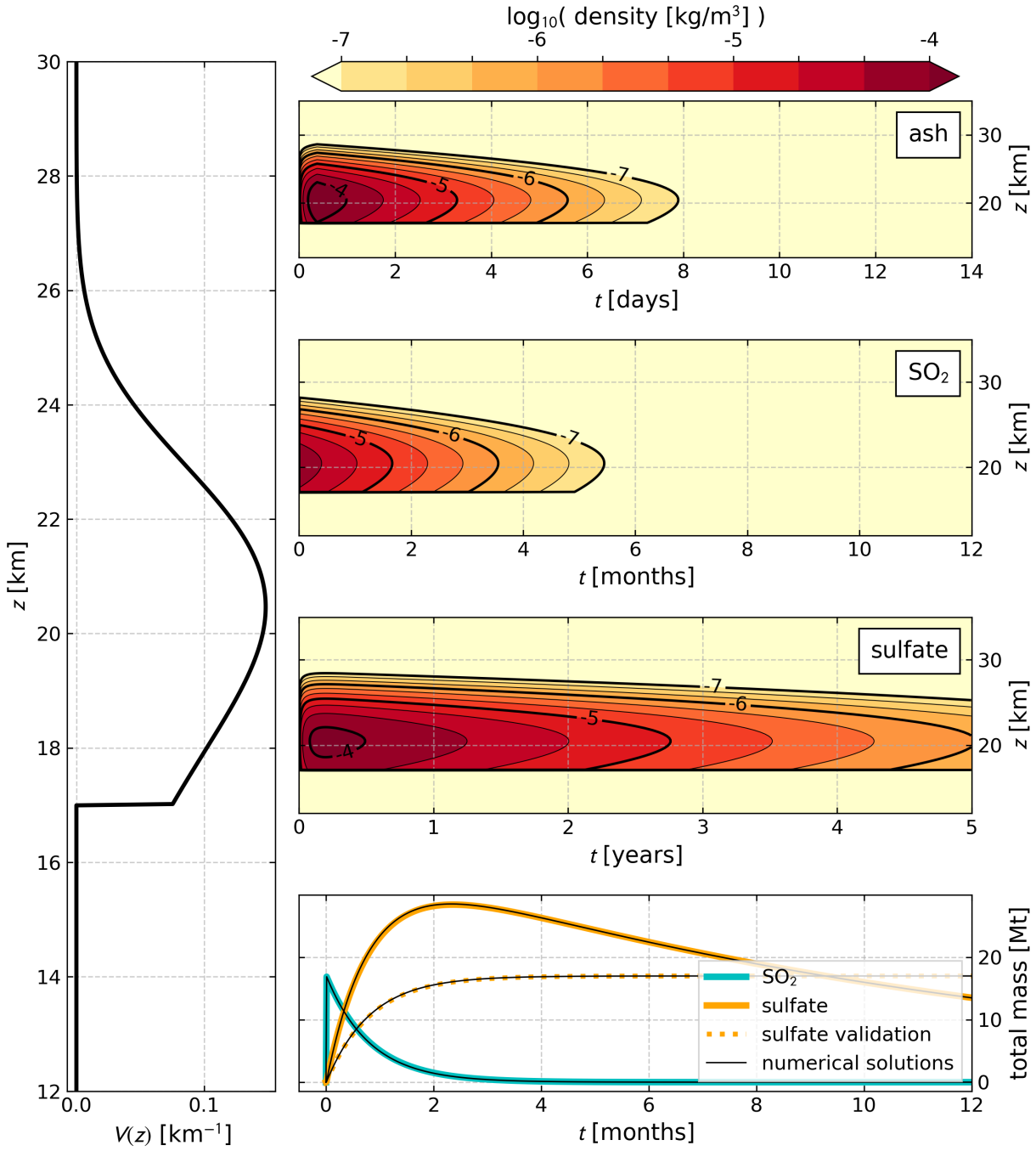

Figure 5: *The analytic (single-column, advection-free) solution to the parameterized injection and $SO_2 \rightarrow$ sulfate reaction given the parameter choices presented in Table 1. (left) the vertical profile Eq.(19) described in Section 2.2. (right) contour plots show the ash, SO_2, and sulfate densities according to Eq.(43), assuming a column area of $a_i = 200^2$ km^2. Differing grid cell areas (resolution) will change the tracer densities in the column, but not the total tracer mass. (bottom right) total SO_2 and sulfate masses according to Eq.(43) and Eq.(48). Also shown is a "sulfate validation" curve, which solves Eq.(46), and conserves the total injected SO_2 mass (see text). Also shown are thin black lines which give numerical (explicit first-order) solutions to the SO_2 and sulfate tendencies, verifying the analytic solutions.*

Eq.(48). The non-decaying sulfate solution Eq.(46) is also shown, providing another visual confirmation that the function balances the SO_2 removal. Figure 4 shows the same total SO_2 and sulfate mass evolution as in Figure 5, with three differing vertical discretizations. This verifies that the normalization is insensitive to this choice, as discussed in Section 2.

2.3 Preliminary results from E3SM

The tracer injection model as described in Section 2.2 has been implemented in E3SMv2 through a routine which is called by the model at each physics grid point, on each physics timestep Δt. On each call, the routine returns the mixing-ratio tendency given by Eq.(25) in kg kg^{-1} s^{-1}, as well as a heating rate in J kg^{-1} s^{-1}, given as the sum of Eq.(28) and (40). These tendencies are then handed to a first-order explicit solver that is used internally by EAMv2 for all physics parameterizations, which updates the fields as

$$q_{j,t+1} = q_{j,t} + \Delta t \frac{\partial q_{j,t}}{\partial t} \tag{49}$$

$$T_{t+1} = T_t + \Delta t \frac{s_{\text{strat}} + s_{\text{surf}}}{c_p} \tag{50}$$

We performed two runs, one with both the stratospheric heating and surface cooling enabled, and one with all tracers behaving passively (both runs include sulfate formation from SO_2), with all parameters otherwise set to their values as shown in Table 1. The runs were both initialized identically from the condition shown in Figure 2. The difference between these two results we call an "anomaly", which is due only to the diabatic heating terms, and is shown in Figure 6 for a period of 6 months post-injection.

Prior to obtaining these outputs, several runs were performed iteratively to tune the heating and cooling rate normalization parameters q^*, τ^* such that the maximum zonal-mean, 1-month time-mean of the heating rates in K/day qualitatively matched Stenchikov et al. (1998) (see their Plate 5) during the month following the injection (peaks values of ~0.3 K/day in the stratosphere, -0.01 K/day at the surface). There, the authors show a plateau in these heating rates for at least 7 months following the injection, while here we see noticeable falloffs by ~5 months. This doesn't seem to be consistent with the sulfate mass loading of the stratosphere, which does persist near it's peak values until the end of the run; the heating implementation will need to be reexamined.

The choice of $z_{\text{AOD}} = 5$ km is also motivated by Plate 5 of Stenchikov et al. (1998), which shows cooling contours of -0.01 K/day as high as 400 hPa, though we note that the surface cooling expression as currently implemented seems to be too weak, and the T anomaly at 500 hPa only varies about zero. Further tuning will be required for a more realistic response.

We also note that the total SO_2 and sulfate masses are about an order of magnitude too low. Unfortunately, debugging efforts have not yet elucidated the cause, and this will be subject to investigation. However, the heating properties of the tracers are independent of this, since the tuning of the normalization parameters q^* and τ^* can always compensate for the discrepancy, in this case yielding realistic global-mean stratospheric temperature anomalies of 3-4 K. We do note, however, that the heating localization appears to peak too low in pressure, and does not coincide with the peak of the vertical injection profile shown in Figure 5. It is doubtful that vertical velocities should be notable enough to cause this; further investigation is pending.

The forcing of the temperature field in this way appears to give rise to shifts in the polar jets; we observe a mean strengthening of the jet in the northern hemisphere (hemisphere of the injection) by ~15 m/s over the second month post-injection. Subsequently, we observe a equator-ward shift of the southern hemisphere polar jet during month 5, suggested by the "dipole" appearing on this feature in the zonal-mean zonal wind. The troposphere and the tropics in general seem to be uninfluenced by these perturbations (again, the surface cooling is currently too weak to be making significant contributions).

Beyond adjustments of the model to address the concerns outlined above, we intend to use our codes to generate ensembles of SAI datasets in this simplified environment, in support of the CLDERA mission. See Section 3.

3 Future work

3.1 Validation of the CLDERA statistical tools

Our immediate next step is to begin to work with the CLDERA pathway detection and attribution tool developers to ingest the model data presented in this report. This will involve the generation of ensembles which will sample the large space of possible pathway realizations. Low-hanging fruit for this purpose are the parameters controlling the strength of the causual relationships which form the idealized pathways; M_{SO2}, k_{SO2},δT_{strat}, δT_{surf}, z_{AOD}, among others. In particular, we intend to produce model

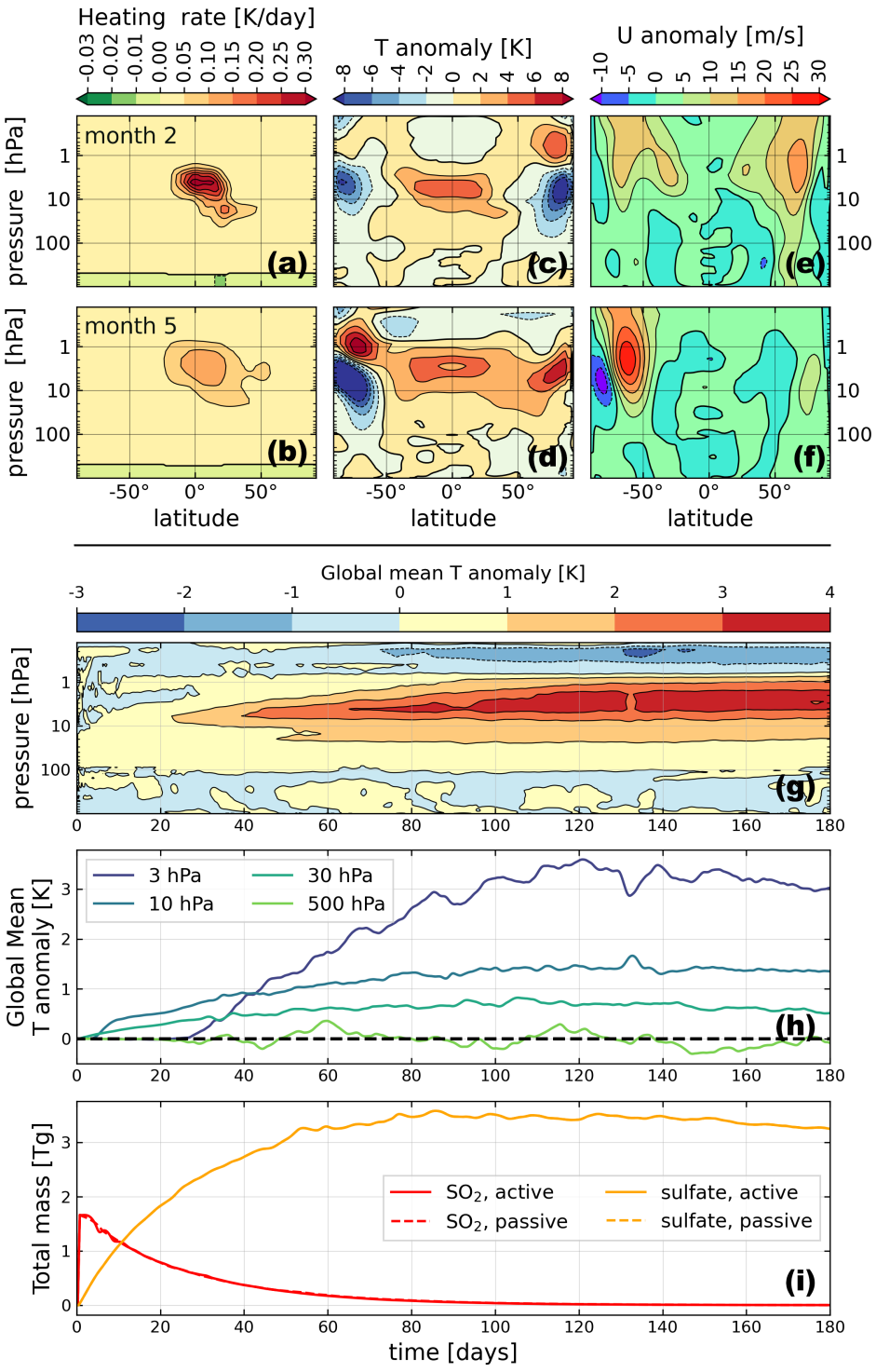

Figure 6: *Difference between two E3SMv2 runs implementing our SAI model, with diabatic enabled and disabled, over a 180-day run. This difference, or "anomaly", shows the temperature and circulation changes due only to the heating of the SAI tracers. See text for a discussion. The six panels near the top of the figure show the zonal-mean time-mean of the local heating rate [(a)-(b)], temperature field [(c)-(d)], and zonal wind [(e)-(f)] over month 2 and month 5 post-eruption. (g): The global-mean temperature anomaly as a function of pressure and time. (h): The global-mean temperature anomaly at selected vertical levels. (i): The total tracer masses over time for SO_2, sulfate.*

outputs for the cases that certain "nodes" of the idealized pathways are either enabled or disabled. For instance:

1. sulfate formation is active, tracers are otherwise passive
2. heating of the stratosphere enabled
3. surface cooling enabled
4. both stratospheric heating and surface cooling are enabled

Further, any of the options 2-4 above can have the active species for the heating and cooling effects be independently chosen. It may also prove valuable to vary the terms related to the localization of the injection (ϕ_0, λ_0, μ,...), since e.g. SAIs in the tropics are expected the have different climate impacts than events of similar magnitude at high latitudes.

It is the hypothesis of the CLDERA project that the automatic discovery of pathways between their sources and its impacts, in a simulated context, will identify etiologically-sound connective relationships. To this end, the members of our generated ensembles will serve as input to verification and validation tests of the statistical pathway discovery and attribution tools. The planned methods that we envision making use of our datasets are described over the following paragraphs.

Global Sensitivity Analysis (GSA) studies the sensitivity of the climate to the injection source terms, and will attempt to establish an "anomaly threshold", below which causal pathways are no longer discernable, and which might be most dominant in impact strength.

Random Forest (RF) Regression, which will learn to create predictive models for climate impact and determine the most important features along the related pathway; the goal of these methods are to narrow the search space by subsequent source attribution efforts.

Software Profiling traces a simulation's "path" through a code, which will leverage E3SMv2's energy "leak checker" infrastructure for detecting changes in global or local physics tendencies in-situ. This method is partially code-invasive, and will have hooks attached to the routines that compute our tracer tendencies as described in this report.

This is only a sub-sample of the methods suggested by the project; as work continues into the next year of the project, the opportunities for these tools to take advantage of our data products should become clear. We suggest that the simple, idealized outputs that we provide will expedite the bridging of the gap between simple statistical tests of these tools, and the perhaps intimidating realm of full-complexity model outputs.

3.2 Further assessments of E3SMv2 stratospheric circulation and stratosphere-troposphere exchange

We intend to perform exhaustive assessments of E3SMv2's stratospheric circulation, and stratosphere-troposphere exchange. This will involve post-processing analyses of the prognostic and diagnostic output fields through transformed Eulerian mean (TEM) investigations (Holton and Hakim, 2013a), and assessments of the realism of notable stratospheric effects such as sudden stratospheric warmings (SSW, Baldwin, Ayarzagüena, et al. (2021)), the quasi-biennial oscillation (QBO, Baldwin, Gray, et al. (2001)), and the tropical "tape recorder" (Mote et al., 1996). Due to it's computational efficiency, we could conceivably apply our HSW configurations for these analyses, as some of these effects are in fact emergent from such an idealized set of forcings (Yao and Jablonowski, 2013; Yao and Jablonowski, 2016). However, we would also like to target outputs from full-complexity runs, such as the E3SMv2 CMIP6 (Eyring, Bony, et al., 2016) outputs.

Another approach we have begun experimenting with is the implementation of new tracer species, the resulting distributions of which are designed as general circulation metrics. This includes the age-of-air (AOA) tracer (Waugh and Hall, 2002), which records the average "age" (or time since last contact with a defined surface layer) of stratospheric air. The distribution of this tracer will converge after a very long spin-up time (at least a decade), after which it will experience perturbations from it's steady-state due to internal variability of the atmosphere, in particular breakdowns of the polar jets (SSWs) associated with tropospheric wave activity (Gupta et al., 2020). We have begun work on this front, and have implemented the necessary tracers into both the CESM2 and E3SMv2 models.

We have also completed preliminary implementations of the "E90" Abalos et al. (2017) and "ST80" (Eyring, Lamarque, et al., 2013) tracers. The E90 tracer is emitted from the surface with a constant flux, and experiences a e-folding decay timescale of 90 days. The ST80 tracer is held at a constant mixing-ratio in the stratosphere (above 80 hPa), and experiences a 25-day e-folding decay

timescale below this threshold. Otherwise, each of these tracers are passive, and their distributions can track meaningful climate metrics e.g. the position of the dynamical tropopause.

The AOA, E90, and ST80 tracers can all be applied just as well to idealized (HSW) configurations of the E3SMv2 model, as well as more those that are more complex. However, the transport of these tracers is of course not a post-processing task, and so we would require nontrivial compute resources to run the more complex model configurations for the lengths of time necessary to gather the relevant statistics (opposed to working with full-complexity datasets that currently exist as the results from large simulation campaigns) . We have confidence that these resources could be obtained through our DOE support.

4 Summary

In this report, we have reviewed the DOE's CLDERA project that seeks to develop methods of automatic attribution of climate impacts to "source" events, e.g. significant geoengineering efforts. The development of tools that deliver this ability is underway, and will require extensive verification and validation, which will be performed under the exemplar source event of the 1991 Mt. Pinatubo volcanic eruption. To this end, we have developed a simplified sub-grid parameterization for the stratospheric injection of volcanic chemical species, their subsequent reactive aerosol products, and climate perturbation by two heating methods (local stratospheric heating, and surface cooling by increased aerosol optical depth). Our physical model for the aerosol evolution is embedded within a highly idealized climatology (a custom-tailored version of the Held-Suarez-Williamson atmospheric forcing) in the DOE E3SMv2 coupled climate model. The parameters of our sub-grid scheme are determined by observation of the 1991 Mt. Pinatubo eruption and subsequent climate evolution, and give promising preliminary results. Future work includes the inclusion of our output data products into the verification and validation suite for the CLDERA project's upcoming pathway discovery and attribution tools, as well as comprehensive evaluation of the E3SMv2 model's stratospheric circulation and stratosphere-troposphere exchange.

5 Acknowledgements

Our group is grateful for funding and scientific support from the DOE and Sandia National Laboratories, namely the leads of the CLDERA project. I thank my advisor Christiane Jablonowski, and all students of the Atmospheric Dynamics Modeling Group's (ADMG) for constant and invaluable collaboration and guidance. Computational resources used for this project were provided by the Cori HPC at the National Energy Research Scientific Computing Center (NERSC) , the Cheyenne HPC the National Center for Atmospheric Research (NCAR), and the University of Michigan's Great Lakes cluster.

References

Abalos, Marta et al. (Oct. 1, 2017). "Using the Artificial Tracer e90 to Examine Present and Future UTLS Tracer Transport in WACCM". In: *Journal of the Atmospheric Sciences* 74.10, pp. 3383–3403. DOI: 10.1175/JAS-D-17-0135.1.

Bader, David et al. (July 11, 2014). *Accelerated Climate Modeling for Energy (ACME) Project Strategy and Initial Implementation Plan — Earth & Environmental Systems Modeling*.

Baldwin, Mark P., Blanca Ayarzagüena, et al. (2021). "Sudden Stratospheric Warmings". In: *Reviews of Geophysics* 59.1, e2020RG000708. DOI: 10.1029/2020RG000708.

Baldwin, Mark P., L. J. Gray, et al. (2001). "The quasi-biennial oscillation". In: *Reviews of Geophysics* 39.2, pp. 179–229. DOI: 10.1029/1999RG000073.

Barnes, John E. and David J. Hofmann (1997). "Lidar measurements of stratospheric aerosol over Mauna Loa Observatory". In: *Geophysical Research Letters* 24.15, pp. 1923–1926. DOI: 10.1029/97GL01943.

Bekki, S. (1995). "Oxidation of volcanic SO2: A sink for stratospheric OH and H2O". In: *Geophysical Research Letters* 22.8, pp. 913–916. DOI: 10.1029/95GL00534.

Bekki, S. and J. A. Pyle (1994). "A two-dimensional modeling study of the volcanic eruption of Mount Pinatubo". In: *Journal of Geophysical Research: Atmospheres* 99 (D9), pp. 18861–18869. DOI: 10.1029/94JD00667.

Bluth, Gregg J. S. et al. (Nov. 1997). "Stratospheric Loading of Sulfur from Explosive Volcanic Eruptions". In: *The Journal of Geology* 105.6, pp. 671–684. DOI: 10.1086/515972.

Bradley, Andrew M., Peter A. Bosler, and Oksana Guba (Sept. 27, 2021). "Islet: Interpolation semi-Lagrangian element-based transport". In: *Geoscientific Model Development Discussions*, pp. 1–48. DOI: 10.5194/gmd-2021-296.

Crutzen, Paul J. (July 25, 2006). "Albedo Enhancement by Stratospheric Sulfur Injections: A Contribution to

Resolve a Policy Dilemma?" In: *Climatic Change* 77.3, p. 211. DOI: 10.1007/s10584-006-9101-y.

Danabasoglu, G. et al. (2020). "The Community Earth System Model Version 2 (CESM2)". In: *Journal of Advances in Modeling Earth Systems* 12.2, e2019MS001916. DOI: https://doi.org/10.1029/2019MS001916.

Dennis, John M. et al. (Feb. 1, 2012). "CAM-SE: A scalable spectral element dynamical core for the Community Atmosphere Model". In: *The International Journal of High Performance Computing Applications* 26.1, pp. 74–89. DOI: 10.1177/1094342011428142.

Eyring, Veronika, Sandrine Bony, et al. (May 26, 2016). "Overview of the Coupled Model Intercomparison Project Phase 6 (CMIP6) experimental design and organization". In: *Geoscientific Model Development* 9.5, pp. 1937–1958. DOI: 10.5194/gmd-9-1937-2016.

Eyring, Veronika, Jean-François Lamarque, et al. (2013). "Overview of IGAC/SPARC Chemistry-Climate Model Initiative (CCMI) Community Simulations in Support of Upcoming Ozone and Climate Assessments". In: p. 19.

Golaz, Jean-Christophe et al. (Apr. 22, 2022). *The DOE E3SM Model Version 2: Overview of the physical model*. Earth and Space Science Open Archive. DOI: 10.1002/essoar.10511174.1.

Guo, Song, Gregg J. S. Bluth, et al. (2004). "Re-evaluation of SO2 release of the 15 June 1991 Pinatubo eruption using ultraviolet and infrared satellite sensors". In: *Geochemistry, Geophysics, Geosystems* 5.4. DOI: 10.1029/2003GC000654.

Guo, Song, William I. Rose, et al. (2004). "Particles in the great Pinatubo volcanic cloud of June 1991: The role of ice". In: *Geochemistry, Geophysics, Geosystems* 5.5. DOI: 10.1029/2003GC000655.

Gupta, Aman, Edwin P. Gerber, and Peter H. Lauritzen (2020). "Numerical impacts on tracer transport: A proposed intercomparison test of Atmospheric General Circulation Models". In: *Quarterly Journal of the Royal Meteorological Society* 146.733, pp. 3937–3964. DOI: 10.1002/qj.3881.

Hannah, Walter M. et al. (2021). "Separating Physics and Dynamics Grids for Improved Computational Efficiency in Spectral Element Earth System Models". In: *Journal of Advances in Modeling Earth Systems* 13.7, e2020MS002419. DOI: 10.1029/2020MS002419.

Held, Isaac M. and Max J. Suarez (Oct. 1, 1994). "A Proposal for the Intercomparison of the Dynamical Cores of Atmospheric General Circulation Models". In: *Bulletin of the American Meteorological Society* 75.10, pp. 1825–1830. DOI: 10.1175/1520-0477(1994)075<1825:APFTIO>2.0.CO;2.

Holasek, R. E., S. Self, and A. W. Woods (1996). "Satellite observations and interpretation of the 1991 Mount Pinatubo eruption plumes". In: *Journal of Geophysical Research: Solid Earth* 101 (B12), pp. 27635–27655. DOI: 10.1029/96JB01179.

Holton, James R. and Gregory J. Hakim (Jan. 1, 2013a). "Chapter 10 - The General Circulation". In: *An Introduction to Dynamic Meteorology (Fifth Edition)*. Ed. by James R. Holton and Gregory J. Hakim. Boston: Academic Press, pp. 325–375. DOI: 10.1016/B978-0-12-384866-6.00010-6.

Holton, James R. and Gregory J. Hakim (Jan. 1, 2013b). "Chapter 12 - Middle Atmosphere Dynamics". In: *An Introduction to Dynamic Meteorology (Fifth Edition)*. Ed. by James R. Holton and Gregory J. Hakim. Boston: Academic Press, pp. 413–452. DOI: 10.1016/B978-0-12-384866-6.00012-X.

Jablonowski, Christiane and David Williamson (2006). "A baroclinic instability test case for atmospheric model dynamical cores". In: *Quarterly Journal of the Royal Meteorological Society* 132.621, pp. 2943–2975. DOI: 10.1256/qj.06.12.

Jablonowski, Christiane and David Williamson (Feb. 8, 2011). "The Pros and Cons of Diffusion, Filters and Fixers in Atmospheric General Circulation Models". In: *Lecture Notes in Computational Science and Engineering*. Vol. 80, pp. 381–493. DOI: 10.1007/978-3-642-11640-7_13.

Lauritzen, P. H. et al. (May 4, 2015). "The terminator "toy" chemistry test: a simple tool to assess errors in transport schemes". In: *Geoscientific Model Development* 8.5, pp. 1299–1313. DOI: 10.5194/gmd-8-1299-2015.

Lin, Shian-Jiann, William Putman, and Lucas Harris (Nov. 28, 2017). "THE GFDL FINITE-VOLUME CUBED-SPHERE DYNAMICAL CORE". In: p. 58.

McCormick, M. Patrick, Larry W. Thomason, and Charles R. Trepte (Feb. 1995). "Atmospheric effects of the Mt Pinatubo eruption". In: *Nature* 373.6513, pp. 399–404. DOI: 10.1038/373399a0.

Mills, Michael J. et al. (Mar. 16, 2016). "Global volcanic aerosol properties derived from emissions, 1990–2014, using CESM1(WACCM)". In: *Journal of Geophysical Research: Atmospheres* 121.5, pp. 2332–2348. DOI: 10.1002/2015JD024290.

Mote, Philip W. et al. (1996). "An atmospheric tape recorder: The imprint of tropical tropopause temperatures on stratospheric water vapor". In: *Journal of Geo-*

physical Research: Atmospheres 101 (D2), pp. 3989–4006. DOI: 10.1029/95JD03422.

Petty, Grant W. (2006). *A first course in atmospheric radiation*. 2nd ed. Madison, Wis: Sundog Pub. xii, 459 p.

Randall, David (Oct. 25, 2010). *The Evolution of Complexity In General Circulation Models*.

Robock, Alan (May 2000). "Volcanic Eruptions and Climate". In: *REVIEWSOF GEOPHYSICS*, p. 29.

Robock, Alan (Feb. 15, 2002). "The Climatic Aftermath". In: *Science* 295.5558, pp. 1242–1244. DOI: 10.1126/science.1069903.

Rosen, James M. (Oct. 1, 1971). "The Boiling Point of Stratospheric Aerosols". In: *Journal of Applied Meteorology and Climatology* 10.5, pp. 1044–1046. DOI: 10.1175/1520-0450(1971)010<1044:TBPOSA>2.0.CO;2.

Self, Stephen et al. (Jan. 1, 1993). "The Atmospheric Impact of the 1991 Mount Pinatubo Eruption". In.

Sheng, J.-X. et al. (Oct. 19, 2015). "A perturbed parameter model ensemble to investigate Mt. Pinatubo's 1991 initial sulfur mass emission". In: *Atmospheric Chemistry and Physics* 15.20, pp. 11501–11512. DOI: 10.5194/acp-15-11501-2015.

Stenchikov, Georgiy et al. (June 27, 1998). "Radiative forcing from the 1991 Mount Pinatubo volcanic eruption". In: *Journal of Geophysical Research* 1031, pp. 13837–13858. DOI: 10.1029/98JD00693.

Tilmes, Simone et al. (Nov. 1, 2018). "CESM1(WACCM) Stratospheric Aerosol Geoengineering Large Ensemble Project". In: *Bulletin of the American Meteorological Society* 99.11, pp. 2361–2371. DOI: 10.1175/BAMS-D-17-0267.1.

Toohey, Matthew et al. (Nov. 11, 2016). "Easy Volcanic Aerosol (EVA v1.0): an idealized forcing generator for climate simulations". In: *Geoscientific Model Development* 9.11, pp. 4049–4070. DOI: 10.5194/gmd-9-4049-2016.

Watts, Jonathan (Dec. 3, 2020). "China plans rapid expansion of 'weather modification' efforts". In: *The Guardian*.

Waugh, Darryn and Timothy Hall (Dec. 2002). "AGE OF STRATOSPHERIC AIR: THEORY, OBSERVATIONS, AND MODELS: AGE OF STRATOSPHERIC AIR". In: *Reviews of Geophysics* 40.4, pp. 1–1–1–26. DOI: 10.1029/2000RG000101.

Williamson, David, Jerry G. Olson, and Byron A. Boville (Apr. 1, 1998). "A Comparison of Semi-Lagrangian and Eulerian Tropical Climate Simulations". In: *Monthly Weather Review* 126.4, pp. 1001–1012. DOI: 10.1175/1520-0493(1998)126<1001:ACOSLA>2.0.CO;2.

Wolfe, Edward W. and Richard P. Hoblitt (1998). "Overview of the Eruptions". In: *Fire and Mud: Eruptions and Lahars of Mount Pinatubo, Philippines*. Univ of Washington Pr.

Yao, Weiye and Christiane Jablonowski (2013). "Spontaneous QBO-like oscillations in an atmospheric model dynamical core". In: *Geophysical Research Letters* 40.14, pp. 3772–3776. DOI: 10.1002/grl.50723.

Yao, Weiye and Christiane Jablonowski (Sept. 1, 2016). "The Impact of GCM Dynamical Cores on Idealized Sudden Stratospheric Warmings and Their QBO Interactions". In: *Journal of the Atmospheric Sciences* 73.9, pp. 3397–3421. DOI: 10.1175/JAS-D-15-0242.1.

Yue, G. K. et al. (1994). "Stratospheric aerosol acidity, density, and refractive index deduced from SAGE II and NMC temperature data". In: *Journal of Geophysical Research: Atmospheres* 99 (D2), pp. 3727–3738. DOI: 10.1029/93JD02989.